

## An Investigation into Metallic Powder Thermal Conductivity in Laser Powder Bed Fusion Additive Manufacturing

Shanshan Zhang<sup>a</sup>, Brandon Lane<sup>b</sup>, Justin Whiting<sup>b</sup>, Kevin Chou<sup>a</sup>

<sup>a</sup>Industrial Engineering, University of Louisville

Louisville, KY, 40292

<sup>b</sup>Engineering Laboratory, National Institute of Standards and Technology

Gaithersburg, MD, 20899

### Abstract

This study investigates the thermal conductivity of metallic powder in laser powder-bed fusion (LPBF) additive manufacturing. The intent is to utilize a methodology combining laser flash testing, finite element (FE) heat transfer modeling, and an inverse method to indirectly measure the thermal conductivity of nickel-based super alloy 625 (IN625) and titanium alloy (Ti64) powder used in LPBF processes. A hollow test specimen geometry was designed and built with LPBF enclosing the un-melted powder to mimic the powder bed conditions. The specimens were then flash heated in a laser flash system to measure their transient temperature response. Next, a developed FE model and a multi-point optimization algorithm were applied to inversely analyze the thermal transient, and extract the thermal diffusivity and conductivity of the powder enclosed in the specimens. The results indicate that the thermal conductivity of IN625 powder used in LPBF ranges from 0.65 W/(m·K) to 1.02 W/(m·K) at 100 °C and 500 °C, respectively. On the other hand, Ti64 powder has a lower thermal conductivity than IN625 powder, about 35 % to 40 % smaller. However, the thermal conductivity ratio of the powder to the respective solid counterpart is not much different between the two materials, about 4 % to 7 %, which is largely temperature independent.

Keywords: laser powder-bed fusion; laser flash; inverse method; thermal properties

### 1. Introduction

Laser powder-bed fusion (LPBF) additive manufacturing (AM) is a process that fabricates parts in a metal powder bed environment by powder-layer spreading and laser heating, melting, and solidifying layer-by-layer. The metal powder bed plays a significant role in the heat transfer phenomenon during LPBF, because heat dissipation to the ambient influences the rate of solidification of the molten metal, and therefore, the microstructure and mechanical properties of the build. In addition, accurate measurement of thermal properties of a powder bed in AM is essential for valid process modeling and predictions. While there are numerous publications regarding the thermal properties of common solid materials, little research has been reported regarding powder thermal properties in AM.

The transient hot-wire method was studied and used by Wei et al. to measure the thermal conductivities of commercial AM metal powders in a pressurized inert gas environment, and the authors reported that the heat dissipation of a powder bed was influenced by gas infiltration [1].

However, Gusarov et al. claimed that the thermal conductivity of gases at ambient pressure is substantially lower than that of metals and considered less important than other factors such as contacts between particles [2]. In addition, many researchers estimated the thermal conductivity of powder in powder-bed fusion AM using numerical approaches. Early work on evaluating the thermal conductivity of composite media can be derived from the Maxwell approach [3-6], which has been improved by the consideration of contacts between neighboring particles and gas in the pores. Some models have been developed to investigate the heat transport mechanism of a powder bed in AM and simulate the effective thermal conductivity. For example, Siu et al. and Slavin et al. both incorporated contact effects, such as the contact angle and the neck area between the neighboring particles for heat transfer in a powder bed, and conducted an analytical study to compute the powder thermal conductivity [7, 8]. Moreover, Singh et al. utilized an artificial neural network approach to predict the effective thermal conductivity of a porous system, which may contribute toward AM powder-bed studies [9]. Gong et al. incorporated powder thermal conductivity obtained from hot-disk based measurements and an analytical means into a 3D finite element (FE) thermal model to simulate the thermal field/history in powder-bed electron beam additive manufacturing [10].

Among different techniques for thermal diffusivity measurements, laser flash analysis, which was first developed by Parker et al. [11], is a widely used method for a wide variety of materials with a high precision. It uses the transient thermal response of a sample after a short heating pulse by a laser, then utilizes various heat transfer models to extract the thermal diffusivity from the measured response. For heterogeneous or anisotropic materials, more complex models may be required. Inverse heat transfer methods, in conjunction with laser flash technique, have been used to evaluate the thermal properties of thin coated films [12-16]. The solution of the analysis in these studies was based on the minimization of the least-squared errors between numerical model predictions and experimentally measured data, which was detailed in a publication from Ozisik [17]. Parker's theory of the flash method assumes one-dimensional heat transfer, without heat losses, and the homogeneity of the tested specimen. On the other hand, it is difficult to measure the thermal conductivity of metal powder, particularly with the size (approximately  $<50\ \mu\text{m}$ ) used in powder-bed fusion. With the inverse method approach, Cheng et al. developed and validated a combined experimental-numerical method to evaluate the powder thermal conductivity using laser flash testing and numerical heat transfer simulations [18]. The authors used additively fabricated hollow samples, with specially designed internal geometry, to enclose powder from LPBF. The internal geometry was designed to overcome an issue in which a gap occurred between the top shell and the internal powder, as reported in [19], which resulted in thermal insulations and complicated heat transport in the testing sample.

Continued from the previous work [18], the objective of this study is to analyze the temperature-dependent thermal conductivity of powder used in LPBF additive manufacturing. The test specimens of different designs, with enclosed powder, were laser-flash heated to obtain experimental thermal response at different temperatures, and the developed inverse methodology was employed to evaluate the temperature-dependent thermal conductivity of both nickel super alloy 625 (IN625) and titanium alloy (Ti64) powder materials.

## 2. Experimental details

### 2.1. Specimen design and fabrication

The test specimens were thin hollow disks built vertically by the LPBF process and to encapsulate powder during fabrication. In addition, internal cone features, either on the top or both the top and bottom sides of the hollow disks were included to ensure the contact between powder and the solid shells, preventing a large-area gap caused by powder settling [19]. As an example, Figure 1(a) is a photo of a fabricated two cones (0.5 mm height) sample. The radial cross-section of the sample model is shown in Figure 1(b). The overall dimensions of hollow disks are 25 mm in diameter and 3 mm in height with a shell of 0.5 mm thickness. The internal geometric feature had three different cone features: (1) both cones with a height of 0.5 mm (noted as 2Cone-0.5 throughout the paper), (2) both cones with a height of 0.25 mm (2Cone-0.25), and (3) one cone with a height of 0.5 mm on the top (1Cone-0.5). The dimensions of the cone-feature designs are shown in Figure 1(c) and Figure 1(d) shows the radial cross-section in the build orientation, i.e., a vertical build.

An EOS M270 system<sup>1</sup> was employed for sample fabrications. The powder materials used included both IN625 and Ti64. To achieve a full-density build, the process parameters suggested by the manufacturer were adopted for the solid shells. For IN625, the process parameter set was 195 W laser power and 800 mm/s scan speed [20] and the layer thickness was set as 40  $\mu\text{m}$ . For Ti64, a laser power of 170 W and a scan speed of 1250 mm/s [21] were used, with a layer thickness of 30  $\mu\text{m}$ . For both materials, the hatch spacing was 100  $\mu\text{m}$ . No laser exposure was applied to the internal hollow section, as it was intended to encapsulate powder.

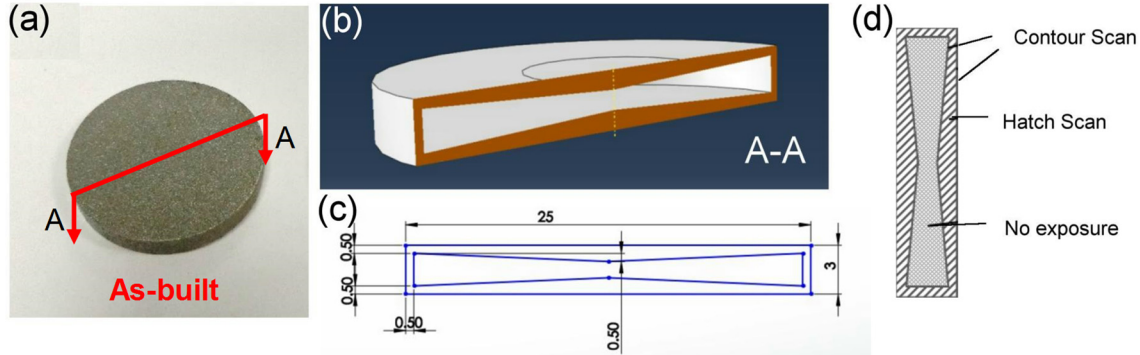


Figure 1. (a) An LPBF fabricated sample; (b) a geometric model of LPBF sample; (c) Dimensions of the 2Cone-0.5 powder-enclosed samples (unit: mm); (d) Build direction and scan conditions in LPBF.

### 2.2. Laser flash testing

Thermal diffusivity measurements of both solid and different encapsulated powder samples were carried out using a DLF-1200 from TA Instruments<sup>1</sup>, shown in Figure 2(a). In this system, the test specimens are held in a furnace chamber, purged with either nitrogen or argon gas, which has environment temperature control that can be increased up to 1600  $^{\circ}\text{C}$ . A laser pulse with a

<sup>1</sup> Certain commercial entities, equipment, or materials may be identified in this document in order to describe an experimental procedure or concept adequately. Such identification is not intended to imply recommendation or endorsement by the National Institute of Standards and Technology, nor is it intended to imply that the entities, materials, or equipment are necessarily the best available for the purpose.

variable energy up to 25 J was applied uniformly in a concentric circular area with a diameter of about 22 mm at the bottom surface of the specimen. The laser power is adjusted and set automatically by the system to create an adequate thermal response and resulting signal from the pyrometer. The duration of laser irradiations was approximately 0.003 s. An infrared pyrometer collects thermal response from a 9.6 mm diameter circular region on the top surface of the test specimen and converts to digital signal output (Figure 2 (b)). To reduce laser reflection, the test specimen was coated with liquid graphite, and dried completely before loading onto a sample holder in the furnace chamber. During testing, the furnace heats to different programmed setpoint temperatures. Once steady state environment temperature is reached, the laser pulses, which increases the sample temperature only enough to enable a measurement from the pyrometer. The procedures and settings of specimen testing suggested by the manufacturer (TA Instruments) were followed.

The laser flash instrument generates a set of thermal radiation measurements collected over time via an infrared pyrometer. The experimentally acquired data is given as the voltage output and then transferred into a normalized response ranging from 0 to 1 which corresponds to the output at lowest and highest signal values. The response vs. time result is termed as a “thermogram.” Since the diffusivity is related to the time response (e.g., rise time of the thermogram), knowledge of the absolute temperature rise due to the laser pulse is not necessary. The experimental results of IN625 and Ti64 are discussed in the following two sections.

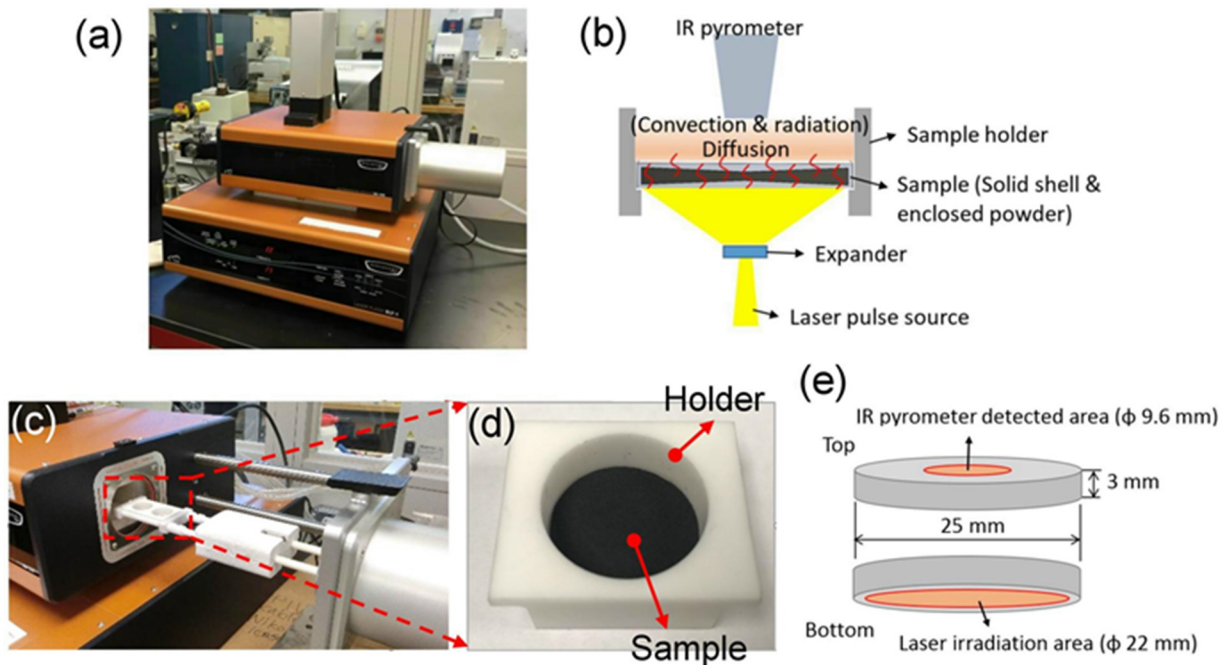


Figure 2. (a) DLF-1200 laser flash apparatus; (b) Schematic of laser flash method; (c) Specimen loading system; (d) Specimen holder; (e) Dimensions of IR detection and laser irradiation areas. Note that pyrometer spot size is not to scale as shown.

### 2.3. IN625 powder samples

Figure 3 shows the experimentally obtained thermograms of a solid sample as well as an example of the 2Cone-0.5 specimen with encapsulated powder. Compared with the solid sample, the heating rate of specimens with encapsulated powder is much slower; the maximum temperature is reached at between 10 s and 20 s vs. less than 3 s for the solid sample. It can also be noticed that as temperature increases, the heating period in the thermogram shifts to the left gradually due to increased thermal diffusivity of the IN625 material with the temperature.

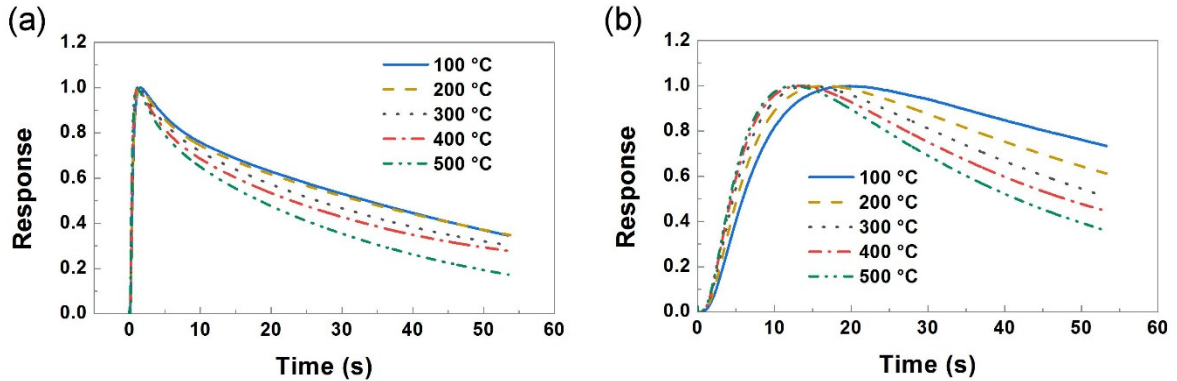


Figure 3. Experimental time-response thermograms of IN625 at various temperatures: (a) solid specimen measurement and (b) specimens with encapsulated powder (2Cone-0.5). Averages are taken from three separate measurements at each temperature.

Furthermore, at a given testing temperature, the thermograms of specimens with 2Cone-0.25 and 1Cone-0.5 features exhibit similar results in the heating period, and on the other hand, the 2Cone-0.5 specimen has a slightly higher heating rate than the specimens with the 2Cone-0.25 feature. An example of the comparison between the three cone features at 100 °C is shown in Figure 4.

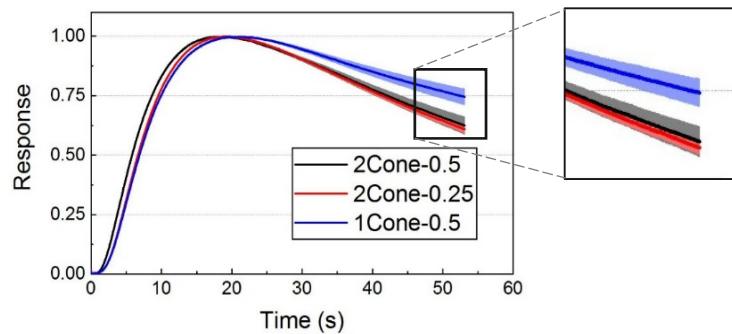


Figure 4. Comparison of laser flash thermograms of IN625 with three cone features at 100 °C. The light-color bars in the plot indicate the range of measurement results.

### 2.4. Ti64 powder samples

Same as the IN625 samples, thermograms from laser flash testing of Ti64 specimens show an increased thermal diffusivity as the testing temperature increases. Figure 5(a) shows the results of the 2Cone-0.5 specimen at various temperatures. Figure 5(b), on the other hand, compares

thermograms from laser flash testing of the IN625 and Ti64 specimens, both with encapsulated powder and with the 2Cone-0.5 feature. It is noted that the Ti64 specimen has slower heating compared to IN625 specimen, indicating a smaller diffusivity value because of the inherently lower thermal diffusivity of Ti64 alloy; in addition, the difference in thermograms between the two materials becomes smaller at higher temperatures.

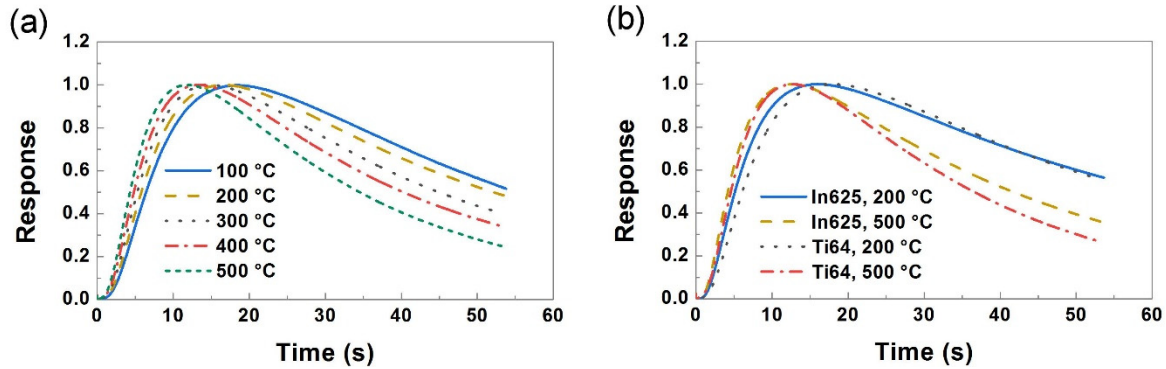


Figure 5. (a) Laser flash thermograms of Ti64 (Ti64) 2Cone-0.5 specimen; (b) Comparison of thermograms between IN625 and Ti64 specimens with encapsulated powder, both with 2Cone-0.5 feature.

### 3. Powder thermal conductivity evaluation

To analyze the thermal conductivity of the powder inside the LPBF-built specimens, the laser flash system was modeled and simulated by a finite element (FE) method using ABAQUS software. The specimen and its holder were modeled using the measured physical dimensions, with a mesh size of 0.5 mm and 0.7 mm, respectively. The laser heat source was simplified as a uniformly-distributed surface heat flux applied on the bottom side of the specimen. Convection and thermal radiation heat loss were included as the boundary conditions with the ambient temperature set as the testing temperature. The encapsulated powder was assumed to have the following unknown properties: density ( $\rho$ ) and conductivity ( $k$ ). Besides, two contact conductance values: (1) between the powder and the top solid shell ( $k_t$ ), and (2) between the powder and the bottom solid shell ( $k_b$ ), needed to be determined as well. Additionally, the specimen-holder contact conductance ( $k_p$ ) at testing temperatures was obtained by analyzing the thermal response of the solid sample testing using the same laser flash system and the FE simulations, and then included in the laser flash simulation for the specimens with encapsulated powder.

Therefore, the problem is to accurately estimate the unknown LPBF powder thermal properties. A multivariate inverse method with a multi-point optimization algorithm was utilized to fit the simulation to the experimental results, and eventually to achieve the powder thermal conductivity in this study. The methodology of the inverse approach uses the Levenberg-Marquardt method, which has been used in a variety of inverse problems [17]. The complete approach, including FE simulations of laser flash testing and the inverse method, is detailed in a previous study [18].



### 3.1. IN625 powder study

In the thermal simulation of laser flash testing, temperature-dependent material properties of solid IN625 [22, 23] and alumina [24], which are applied for the solid capsule of the sample and the sample holder, respectively, are given in Figure 6. In addition, the density of alumina is assumed as  $3800 \text{ kg/m}^3$  [25]. Moreover, the emissivity (unitless) for IN625 and alumina is 0.12 to 0.16 [26] and 0.7 [24], respectively. The convection coefficient was estimated to be  $10 \text{ W}/(\text{m}^2\cdot\text{K})$  [27]. The uncertainty of these assumed parameters is assumed to have an insignificant effect on the evaluation of the unknown parameters determined by the inverse method (e.g., powder thermal conductivity), although the sensitivity to parameter uncertainty is yet to be studied.

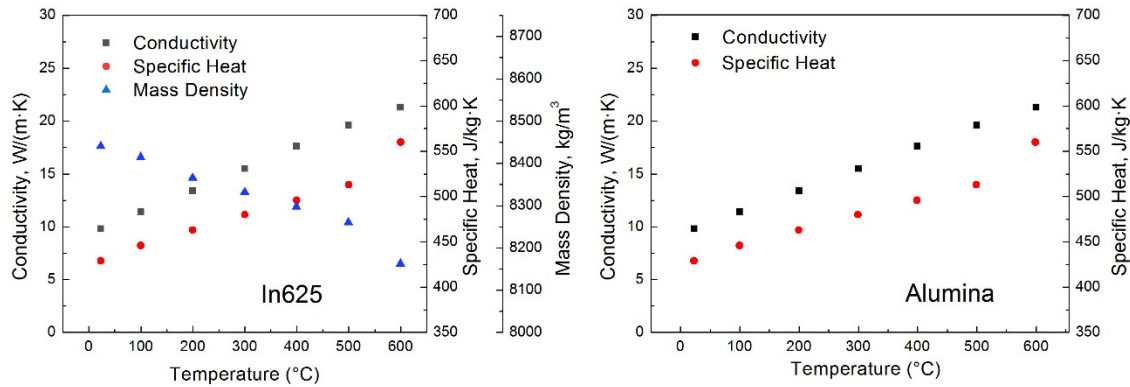


Figure 6. Material properties of solid IN625 sample and alumina sample holder.

#### 3.1.1. Example of powder-enclosed sample analysis

Figure 7(a) shows the thermograms from three shots of laser flash testing of an IN625 specimen (2Cone-0.5) at  $100 \text{ }^\circ\text{C}$ . To illustrate iterative results from the inverse method, Figure 7(b) shows the simulated thermogram from each iteration, with the third and fourth approaching the experimental curve. Table 1 below lists the simulations output as well as the overall error (S), calculated as the sum-squared error between the measured and simulated thermogram, calculated at each iteration. The initial values for the four unknowns were set as 10 % of the solid IN625 density and thermal conductivity at the testing temperature, and  $100 \text{ W}/(\text{m}^2\cdot\text{K})$  for the contact conductance. The initials were purposely set far away from the possible actual values to ensure no effects of initials to the final solution. By adjusting the damping factor in each iteration [18], an optimal set of the four unknown properties was selected for the next step. By calculating the S value (overall error), it can be determined if the simulation for the next iteration is necessary to proceed. In this case, the result from the 3<sup>rd</sup> iteration is considered the optimal solution, because the error increases at the 4<sup>th</sup> iteration.

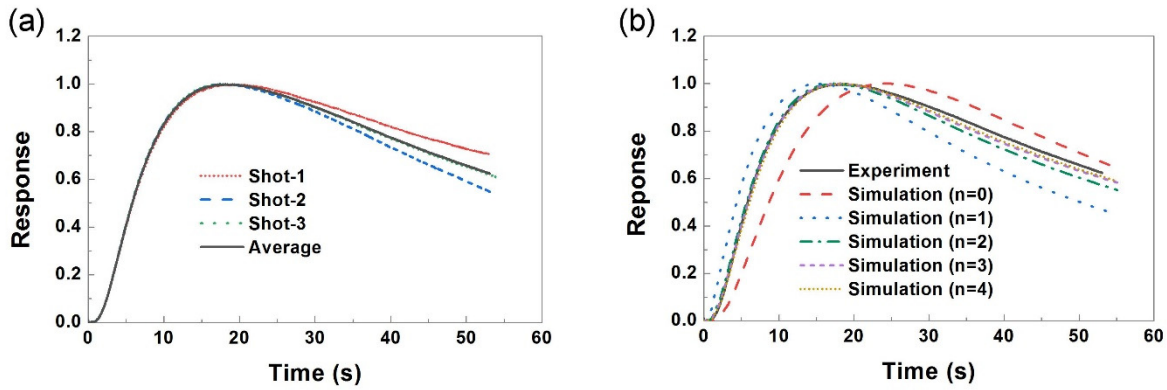


Figure 7. (a) Experimental results, including three shots and the average thermogram, and (b) Simulated thermograms from each iteration.

Table 1. Results from inverse method for IN625 2Cone-0.5 specimen at 100 °C.

n	Damping factor $u$	$k_s$ , W/(m·K)	$k_t$ , W/(m <sup>2</sup> ·K)	$k_b$ , W/(m <sup>2</sup> ·K)	$\rho$ , kg/m <sup>3</sup>	$S$
0		0.1	100	100	841	0.512417
1	-2	0.4314	609.90	566.95	902.63	0.275936
2	-0.02996	0.7347	372.60	738.03	3682.66	0.015569
3*	0.05	0.7955	351.77	926.54	4775.56	0.003393
4	-9.2	0.8000	351.62	934.50	4740.68	0.003789

\* Optimal solution

### 3.1.2. Temperature-dependent thermal conductivity

The laser flash results of the IN625 specimens with encapsulated powder, and three different cone features, at various temperatures were analyzed to inversely calculate the temperature-dependent powder conductivity. The results are summarized in Figure 8. The powder conductivity obtained ranges from 0.65 W/(m·K) to 1.02 W/(m·K), and generally, the powder conductivity is nearly linear to the temperature. However, the results extracted from the samples of three different cone features are slightly different. The models of the 2Cone-0.25 and 1Cone-0.5 give a similar powder thermal conductivity, while the powder conductivity analyzed from the 2Cone-0.5 model is about 0.1 W/(m·K) to 0.2 W/(m·K) higher than that from the other two models for all testing temperatures.



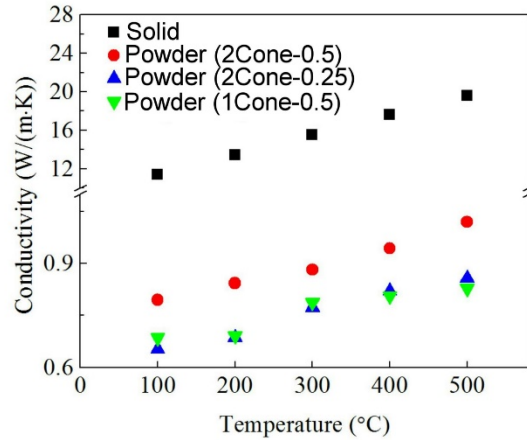


Figure 8. Thermal conductivity of IN625 powder.

### 3.2. Ti64 powder study

The FE model for Ti64 specimens with encapsulated powder was established also based on the actual geometry of fabricated specimens and Ti64 material properties. Figure 9 shows the material properties of solid Ti64 [28] that were incorporated in FE modeling. The same simulation approach and the inverse method used in the IN625 powder study were employed to the Ti64 2Cone-0.5 specimens with encapsulated powder.

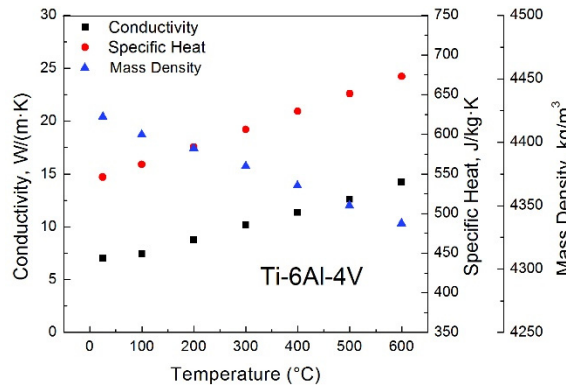


Figure 9. Thermal properties of solid Ti64.

The analyzed thermal conductivity values of Ti64 powder at various temperatures (100 °C to 500 °C) are plotted in Figure 10(a). It can be observed that the simulated Ti64 powder thermal conductivity linearly increases with temperatures and ranges from 0.39 W/(m·K) to 0.65 W/(m·K), for 100 °C and 500 °C, respectively. Moreover, when plotting in a normalized way (i.e., in reference to solid), it is noted that the Ti64 powder conductivity is approximately only 4 % to 5 % of the solid Ti64 conductivity at all testing temperatures, Figure 10(b). This finding is similar to the results of IN625 powder, which shows a slightly higher ratio, 4 % to 7 %, and different cone configurations result in a minor difference.

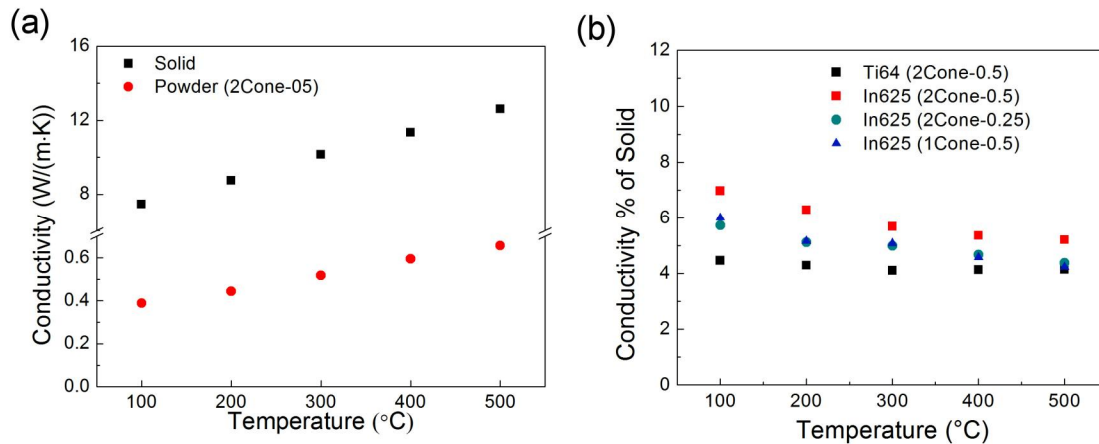


Figure 10. (a) Thermal conductivity of Ti64 powder at different temperatures, and (b) ratio of powder to solid thermal conductivities for IN625 and Ti64 (Ti64).

#### 4. Conclusions

The LPBF specimens with encapsulated powder were designed and fabricated, to imitate powder-bed conditions in LPBF, by an EOS M270 system using two different powder materials: IN625 and Ti64. Different internal cone features were incorporated in the specimens to ensure contact between the powder and the top solid shell. To evaluate the powder thermal conductivity, laser flash experiments and a numerical approach using FE thermal simulations and an inverse method were conducted to analyze the powder thermal conductivity.

Based on the results obtained so far, it can be concluded that (1) the thermal conductivity of powder from LPBF is much lower than the solid conductivity, e.g., 0.65 W/(m·K) to 1.02 W/(m·K) for IN625, and 0.39 W/(m·K) to 0.65 W/(m·K) for Ti64, within the range of measured temperatures of 100 °C to 500 °C, (2) there is a linear correlation between the powder thermal conductivity value and the temperature, and (3) on the other hand, the powder thermal conductivity of both materials is approximately only 4 % to 7 % of their solid thermal conductivity, with Ti64 at a lower ratio.

#### 5. Acknowledgements

This study is supported by National Institute of Standards and Technology (NIST) (CA No. 70NANB16H029). Discussions with and suggestions from Dr. Alkan Donmez are highly appreciated. The authors also acknowledge the technical support from Rapid Prototyping Center and the computational resource from Cardinal Research Cluster at University of Louisville.

#### 6. References

1. Wei, L.C., L.E. Ehrlich, M.J. Powell-Palm, C. Montgomery, J. Beuth, and J.A. Malen, *Thermal conductivity of metal powders for powder bed additive manufacturing*. Additive Manufacturing, 2018. **21**: p. 201-208.
2. Gusarov, A., T. Laoui, L. Froyen, and V. Titov, *Contact thermal conductivity of a powder bed in selective laser sintering*. International Journal of Heat and Mass Transfer, 2003. **46**(6): p. 1103-1109.

3. Maxwell, J.C., *A treatise on electricity and magnetism*. Vol. 1. 1881: Clarendon press.
4. Nan, C.-W., R. Birringer, D.R. Clarke, and H. Gleiter, *Effective thermal conductivity of particulate composites with interfacial thermal resistance*. Journal of Applied Physics, 1997. **81**(10): p. 6692-6699.
5. Mercier, S., A. Molinari, and M. El Mouden, *Thermal conductivity of composite material with coated inclusions: applications to tetragonal array of spheroids*. Journal of Applied Physics, 2000. **87**(7): p. 3511-3519.
6. Gu, G. and Z. Liu, *Effects of contact resistance on thermal conductivity of composite media with a periodic structure*. Journal of Physics D: Applied Physics, 1992. **25**(2): p. 249.
7. Siu, W. and S.-K. Lee, *Effective conductivity computation of a packed bed using constriction resistance and contact angle effects*. International journal of heat and mass transfer, 2000. **43**(21): p. 3917-3924.
8. Slavin, A.J., F.A. Londry, and J. Harrison, *A new model for the effective thermal conductivity of packed beds of solid spheroids: alumina in helium between 100 and 500 C*. International Journal of Heat and Mass Transfer, 2000. **43**(12): p. 2059-2073.
9. Singh, R., R. Bhoopal, and S. Kumar, *Prediction of effective thermal conductivity of moist porous materials using artificial neural network approach*. Building and Environment, 2011. **46**(12): p. 2603-2608.
10. Gong, X., B. Cheng, S. Price, and K. Chou. *Powder-bed electron-beam-melting additive manufacturing: powder characterization, process simulation and metrology*. in *Proceedings of the ASME District F Early Career Technical Conference*. 2013.
11. Parker, W., R. Jenkins, C. Butler, and G. Abbott, *Flash method of determining thermal diffusivity, heat capacity, and thermal conductivity*. Journal of applied physics, 1961. **32**(9): p. 1679-1684.
12. Stryczniewicz, W. and A.J. Panas, *Numerical data processing from a laser flash experiment on thin graphite layer*. Computer Assisted Methods in Engineering and Science, 2017. **22**(3): p. 279-287.
13. Wright, L., X.-S. Yang, C. Matthews, L. Chapman, and S. Roberts, *Parameter estimation from laser flash experiment data*, in *Computational Optimization and Applications in Engineering and Industry*. 2011, Springer. p. 205-220.
14. McMasters, R.L., R.B. Dinwiddie, and A. Haji-Sheikh, *Estimating the thermal conductivity of a film on a known substrate*. Journal of Thermophysics and Heat Transfer, 2007. **21**(4): p. 681-687.
15. Kim, S.-K. and Y.-J. Kim, *Determination of apparent thickness of graphite coating in flash method*. Thermochemica Acta, 2008. **468**(1-2): p. 6-9.
16. Cernuschi, F., L. Lorenzoni, P. Bianchi, and A. Figari, *The effects of sample surface treatments on laser flash thermal diffusivity measurements*. Infrared physics & technology, 2002. **43**(3-5): p. 133-138.
17. Ozisik, M.N., *Inverse heat transfer: fundamentals and applications*. 2000: CRC Press.
18. Cheng, B., B. Lane, J. Whiting, and K. Chou, *A Combined Experimental-Numerical Method to Evaluate Powder Thermal Properties in Laser Powder Bed Fusion*. Proceedings of the ASME 2018 13th International Manufacturing Science and Engineering Conference, 2018, TX, USA, 2018.
19. Whiting, J., B. Lane, K. Chou, and B. Cheng, *Thermal property measurement methods and analysis for additive manufacturing solids and powders*. Proceedings of the 28th International Solid Freeform Fabrication Symposium. Austin, TX, USA, 2017.

20. Anam, M.A., J. Dilip, D. Pal, and B. Stucker. *Effect of scan pattern on the microstructural evolution of Inconel 625 during selective laser melting*. in *Proceedings of 25th Annual International Solid Freeform Fabrication Symposium*. 2014.
21. Zhang, S., *Design, analysis, and application of a cellular material/structure model for metal based additive manufacturing process*. 2017.
22. Capriccioli, A. and P. Frosi, *Multipurpose ANSYS FE procedure for welding processes simulation*. *Fusion engineering and Design*, 2009. **84**(2-6): p. 546-553.
23. *Inconel 625 material properties*. Available from: <http://www.hightempmetals.com/techdata/hitempInconel625data.php>. Accessed October 10, 2017.
24. Han, Q., R. Setchi, S.L. Evans, and C. Qiu, *Three-dimensional finite element thermal analysis in selective laser melting of Al-Al<sub>2</sub>O<sub>3</sub> powder*.
25. Vora, H.D. and N.B. Dahotre, *Multiphysics theoretical evaluation of thermal stresses in laser machined structural alumina*. *Lasers in Manufacturing and Materials Processing*, 2015. **2**(1): p. 1-23.
26. Angela, J., Z. Radovan, and P. Frantisek, *Archives of Mechanical Technology and Materials*.
27. Cheng, B., S. Shrestha, and K. Chou, *Stress and deformation evaluations of scanning strategy effect in selective laser melting*. *Additive Manufacturing*, 2016. **12**: p. 240-251.
28. Yang, J., S. Sun, M. Brandt, and W. Yan, *Experimental investigation and 3D finite element prediction of the heat affected zone during laser assisted machining of Ti6Al4V alloy*. *Journal of Materials Processing Technology*, 2010. **210**(15): p. 2215-2222.